Macromolecules
ARTICLE

Macromolecules **2010**, *43*, 5075–5082 **5075**
DOI: 10.1021/ma100476s

Microscopic Structure Analysis of Clay−Poly(ethylene oxide) Mixed Solution in a Flow Field by Contrast-Variation Small-Angle Neutron Scattering

Takuro Matsunaga, Hitoshi Endo, Makiko Takeda, and Mitsuhiro Shibayama*

Institute for Solid State Physics, The University of Tokyo, 5-1-5 Kashiwanoha, Kashiwa, Chiba 277-8581, Japan

Received March 1, 2010; Revised Manuscript Received April 27, 2010

ABSTRACT: The microscopic structures of clay−polymer aqueous solutions under shear deformation were investigated by means of small-angle neutron scattering (SANS). Laponite (clay) platelet dispersions in poly(ethylene oxide) (PEO) aqueous solutions with various deuterious/hydrogeneous water compositions were prepared, and contrast-variation SANS experiments were carried out. Reversible shear-thinning behaviors were observed in both clay dispersions and PEO solutions. No anisotropy was observed in SANS patterns even though clay platelets are highly anisotropic, indicating rotation of platelets in a shear flow. In the presence of PEO, on the other hand, a strong anisotropic SANS pattern was observed in the shear flow. This suggests that clay platelets are embedded in a cloud of PEO chains and the cloud is elongated along the shear flow direction by shearing, resulting in a strong clay orientation. Contrast-variation SANS clearly exhibited shear-induced adsorption−desorption of polymer chains on the clay surface.

Introduction

It is known that by adding polymer to suspension of colloidal particles the stability of colloids changed and the mixed solution showed a variety of rheological behaviors, such as shear-induced ordering, disordering, thinning, and thickening.[1−3] These nanocomposite materials have attracted the interest of a number of researchers and widely used as various materials, e.g., plastic fiber, food, cosmetics, paints, soap, etc.[4−6] Recently, nanocomposite gels have been gathering much attention because of their many combinations and variety of novel properties.[7,8] Schexnailder and Schmidt highlighted recent accomplishments and their trends of nanocomposite polymer hydrogels with a focus on creative approaches to generating structures, properties, and functions.[9]

Among a variety of combinations of polymers and colloidal particles, the combination of clay and poly(ethylene oxide) (PEO) systems has been gathering much attention in recent years, and many studies have been reported.[10−13] For example, Lal and Auvray first attempted to observe the thickness of adsorbed polymer layer on the clay by contrast matching method.[14,15] Schmidt et al. carried out simultaneous measurements of the structure and rheological properties by small-angle neutron scattering (SANS) coupled with a rheometer and observed a preferential orientation of clay along to the shear direction.[16−18] Lisi and co-workers investigated the relationship between rheological properties and structure of clay and PEO or poly(propylene oxide) oligomers and reported that clay platelets are coated by polymer chains and interact with each other by repulsive or attractive interactions depending on the molecular weight of PEO.[13] Loizou et al. reported molecular weight and concentration dependence of the rheological properties and orientational behavior of PEO−clay aqueous solutions. By shear deformation, large-scale inhomogeneities rolled up and clay platelets oriented with their long axis parallel to the neutral direction.[19,20]

*To whom correspondence should be addressed: Ph +81-4-7136-3418; Fax +81-4-7134-6069; e-mail sibayama@issp.u-tokyo.ac.jp.

PEO−clay aqueous solutions are three-component systems. In order to fully understand such a three-component system by small-angle neutron scattering (SANS), it is inevitable to decompose a SANS intensity function to six partial structure factors, i.e., three self-terms, $S_{ii}(q)$ and three cross-terms, $S_{ij}(q)$, where i and j denote the component such as A, B, and C. However, most studies in the literature simply used (i) deuterated solvent or (ii) contrast-matched solvent. In the case of (i), the information on structures of clay and polymer cannot be separated. In the case of (ii), on the other hand, the contrast matching technique allows to decompose clay scattering, $S_{CC}(q)$, and polymer scattering, $S_{PP}(q)$. However, information about the clay−polymer interface is still missing. Endo et al. developed a contrast-variation method coupled with a singular value decomposition of scattering intensities. This method allows extraction of all of the necessary structure factors to understand multicomponent system. Endo and co-workers successfully used this method to investigate the role of block copolymer additives for calcium carbonate crystallization.[21]

We have investigated the structure of poly(*N*-isopropylacrylamide) (PNIPA) clay nanocomposite gels by using the contrast-variation small-angle neutron scattering (CV-SANS) method in both isotropic and uniaxially deformed states, which allows us to decompose the scattering intensity not only to self-terms, $S_{CC}(q)$ and $S_{PP}(q)$, but also to cross-terms, $S_{ij}(q)$, where i and j denote the component C (clay) or P (polymer).[22,23] In this study, we carried out a rheo-SANS measurement, i.e., an in situ measurement of SANS and rheology, to elucidate the structural changes in a mixture of clay and PEO aqueous solutions and the degree of orientation of clay and polymer chains.

Theoretical Background

1. Clay Orientation in a Shear Flow. First of all, let us make a thought experiment of clay orientation in a shear flow and expect scattering patterns. Figure 1 schematically shows an overview of a rheo-SANS experiment: (a) overview of the

Published on Web 05/12/2010

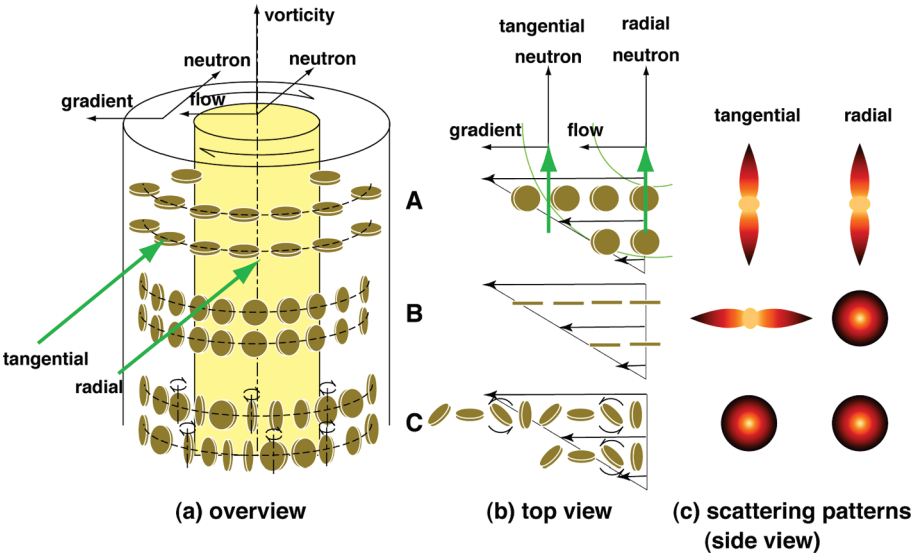

Figure 1. Schematic representation of rheo-SANS on clay−PEO aqueous solutions: (a) overview of the optical setup, (b) top view, and (c) scattering patterns (side view).

optical setup, (b) top view, and (c) scattering patterns (side view). Here, a Couette rheometer (a double-cylinder-type rheometer) is used. The inner and outer cylinders are a rotor and a stator, respectively. The vorticity direction is taken perpendicular to the incident beam direction. There are two ways to shoot the incident beam to the rheometer, i.e., the radial and the tangential setups. In the case of the radial setup, the flow (shear) direction is perpendicular to the beam, while the tangential setup means parallel orientation of the flow direction to the incident beam. Let us consider the case that nanometer-order thin platelets are floated in a shear field. There are three ways of clay orientation in the flow. Parallel orientation of the platelet axis to the vorticity direction (type A), perpendicular orientation (type B), and autorotation due to the shear flow (type C). In type A, the platelets may autorotate by keeping its axis parallel to the vorticity. Type B may unlike to occur because the shear flow leads to platelet rotation, resulting in the type C movement. In particular, if the clay platelets are surrounded by polymer chains, autorotation would be strongly suppressed. As a matter of fact, Schmidt et al. observed a pattern of type A.[16] In the following section, we derive the scattering function based on the above-discussed clay orientation.

2. Contrast-Variation SANS (CV-SANS) and the Partial Scattering Functions. In the case of ternary systems (i.e., clay, polymer, and solvent), the scattering intensities, $I(q)$, are described with three partial scattering functions, $S_{ij}(q)$

$$I(q) = \Delta\rho_C{}^2 S_{CC}(q) + 2\Delta\rho_C\Delta\rho_P{}^2 S_{CP}(q) + \Delta\rho_P{}^2 S_{PP}(q) \quad (1)$$

where $\Delta\rho_i$ indicates the difference of scattering length density between the component i and the water (with i = C and P for clay and polymer, respectively). $S_{CC}(q)$ and $S_{PP}(q)$ are the self-terms of each component, and $S_{CP}(q)$ is the cross-term between clay and polymer. In CV-SANS, a cross-term is very important, and it directly indicates the interaction between the two components. The detailed theoretical as well as experimental description of CV-SANS is given elsewhere.[21]

3. Calculation of the Form Factors. Let us define the laboratory and sample coordinates of the systems O-xyz and O-$x_1y_1z_1$, respectively.[24] Here, the incident beam direction is taken as x axis and the vorticity direction as y axis. The z axis can be either flow direction (radial setup) and gradient direction (tangential setup). Thin disks with the radius R_c and the thickness D_c are preferentially oriented with its axial direction z_1 in the direction of (α, Ω) with respect to the laboratory axis z as shown in Figure 2, where α and Ω are the polar and azimuthal angles, respectively. The incident neutron beam propagates along the x-direction. The flow direction is parallel to the z-direction when the axis of rotation is taken along O-y axis as shown in Figure 2b. In this case, the scattering vector q is given by

$$\begin{aligned} q_x &= -q(\sin\mu\sin\Omega\cos\alpha - \cos\mu\sin\alpha) \\ q_y &= -q\sin\mu\cos\Omega \\ q_z &= -q(\sin\mu\sin\Omega\sin\alpha + \cos\mu\cos\alpha) \end{aligned} \quad (2)$$

Here, q is the magnitude of the scattering vector $q \equiv (4\pi/\lambda)\sin\theta$ and 2θ is the scattering angle. The scattering amplitude, $A_{disk}(q;R_C,D_C;\alpha,\Omega)$, is given by

$$A_{disk}(q;R_C,D_C;\alpha,\Omega) = V_C\frac{\sin\{q_z(D_C/2)\}}{q_z(D_C/2)}\frac{2J_1(\sqrt{q_x{}^2+q_y{}^2}R_C)}{\sqrt{q_x{}^2+q_y{}^2}R_C} \quad (3)$$

Here, V_C is the volume of the disk, i.e., $V_C = \pi R_C{}^2 D_C$. Since the disks are randomly oriented with respect to z, A_{disk} becomes

$$A_{disk}(q;R_C,D_C;\alpha) = V_C\frac{\sin\{qD_C/2)\cos\alpha\}}{q(D_C/2)\cos\alpha}\frac{2J_1(qR_C\sin\alpha)}{qR_C\sin\alpha} \quad (4)$$

and the form factor $P_{disk}(q;R_C,D_C;\alpha) = P_{CC}(q)$ is written by

$$P_{CC}(q) = \frac{n_C}{2}\int_{\alpha=0}^{\pi} A_{disk}(q;\alpha)^2\sin\alpha\,d\alpha \quad (5)$$

n_C is the number density of the disks, i.e., $n_C = \phi_{disk}/V_C$, with the volume fraction of the disk, ϕ_{disk}. The disks are covered with a polymer-adsorbed layer with its volume fraction of

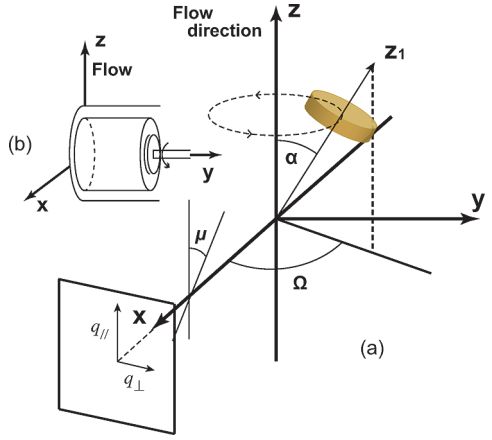

Figure 2. Coordinate system of a disk with radius R and length $2D$ in a Couette shear flow.

ϕ_{pl}. As a result, the radius and the thickness of the disk become R_{pl} and D_{pl}.

$$P_{CP} = \frac{n_C}{2}(\phi_{pl} - \phi_{pex}) \int_{\alpha=0}^{\pi} A_{disk}(q; R_C, D_C; \alpha) A_{disk}(q; R_{pl}, D_{pl}, \alpha) \sin\alpha \, d\alpha - \frac{n_C}{2}\phi_{pl} \int_{\alpha=0}^{\pi} A_{disk}(q; R_{pl}, D_{pl}, \alpha)^2 \sin\alpha \, d\alpha \quad (6)$$

ϕ_p, ϕ_{pl}, ϕ_{pex}, R_{pl}, and D_{pl} mean the volume fraction of PEO, the local volume fraction of PEO layer on clay, the volume fraction of polymer which is not adsorbed on clay platelets, the radius, and the thickness of PEO layer which includes clay. The medium surrounding the disks is filled with polymer solutions with its volume fraction of ϕ_{pex}.

$$P_{PP} = \frac{n_C}{2} \int_{\alpha=0}^{\pi} [(\phi_{pl} - \phi_{pex}) A_{disk}(R_{pl}, D_{pl}, \alpha) - \phi_{pl} A_{disk}(R_C, D_C, \alpha)]^2 \sin\alpha \, d\alpha + \frac{S^0{}_{PP}(0)}{1 + \xi^2 q^2} \quad (7)$$

The scattering function of the polymer matrix is assumed to be that of semidilute polymer solution, i.e., Ornstein−Zernike (OZ) equation with the correlation length, ξ. This model was employed in our previous studies and Miyazaki et al. for randomly oriented systems neglecting the interdisk interference.[25]

The incoming neutron beam is scattered by the sample and the scattering intensity is detected on the area detector

$$q_{para} = q_z \qquad q_{perp} = q_y \quad (8)$$

$$I(q_{para}, q_{perp}) = \frac{\int_0^{\pi/2} W(\alpha) I_{disk}(q; \alpha, \mu) \sin\alpha \, d\alpha}{2\pi \int_0^{\pi/2} W(\alpha) \sin\alpha \, d\alpha} \quad (9)$$

where $W(\alpha)$ is the orientation function with respect to the z-axis. Here μ is the azimuthal angle on the detector. When a flow field is not applied, the clay is oriented randomly and the scattering intensity is isotropic and is given by $I(q_{para}, q_{perp}) = I(q)$. On the other hand, by applying a shear flow with its vorticity direction along to the y-direction, the scattering intensity becomes anisotropic. When the disk is in a flow field, the disk is oriented preferentially with its axis z_1 parallel to the vorticity direction as shown in Figure 2b. Hence, the orientation function can be given by

$$W(\alpha) = \begin{cases} 0 & 0 \le \alpha < \alpha_C \\ 1 & \alpha_C < \pi/2 \end{cases} \quad (10)$$

where α_C is the cutoff angle. The interdisk interference is given by Percus−Yevick function with the radius R_{PY} as employed by Endo et al. for randomly oriented systems and by Nishida et al. for preferentially oriented system.[23] $S_{CC}(q)$ is composed of structure factor of cylinder and form factor of Percus−Yevick potential with the Percus−Yevick radius of clay, R_{PY}.[26]

Experimental Section

1. Samples. Poly(ethylene oxide) (PEO) of the molecular weight being M_V = 1000 kg/mol was purchased from Aldrich Co., Ltd., where M_V is the viscosity-average molecular weight. Synthetic clay Laponite XLG ($[Mg_{5.34}Li_{0.66}Si_8O_{20}(OH)_4]Na_{0.66}$) (Rockwood Ltd.) was purified by dispersion and sedimentation with 70% isopropyl alcohol and deionized water mixture several times, followed by the same procedure with 70% ethanol and water mixture. PEO and clay were mixed in a mixture of deionized water (Direct-Q; Millipore Co. Ltd.) and heavy water (reagent grade, 99.9%) by stirring. A viscoelastic solution consisted of 1.15 vol % clay and 1.81 vol % of PEO was prepared by vigorous stirring with a magnetic stirrer until well-blended at room temperature. It is noted that the radius and thickness of clay are known to be 150 and 10 Å, respectively.[27] Thus, prepared samples were stored for 2 days before rheological and SANS experiments were conducted in order to reduce any effect by time-dependent structure organization.

2. Rheological Measurement. Rheological measurements were carried out on an MCR-501 (Anton Paar, Physica, Austria) with cone−plate type cell as well as double cylinder type cell at 25 °C. The diameters of the outer and the inner cylinders were 50.0 and 48.0 mm, respectively, and the gap was 1.00 mm. The radius of the cell was 25.0 mm, and the cone angle was 0.99°.

3. Rheo-SANS. A Rheo-SANS was carried out with MCR-501 on the SANS diffractometer, SANS-U, Institute for Solid State Physics, The University of Tokyo.[28,29] The wavelength of incident neutrons was λ = 7.0 Å (±10%), and the sample-to-detector distances (SDD) were 2 and 8 m. This setup allowed us to obtain SANS intensity functions, $I(q)$, in the range of $0.005 \le q \le 0.2$ Å^{-1}. Here, q is the magnitude of the scattering vector, i.e., $q \equiv (4\pi/\lambda) \sin\theta$, where 2θ is the scattering angle. A double-cylinder type shear cell made of quartz was used for SANS. The diameters of the outer and the inner cylinders were the same as described above, i.e., 50.0 and 48.0 mm, respectively, and the gap was 1.00 mm. Two-dimensional (2D) profiles along the radial and the tangential directions were obtained under a shear flow. Here, the radial and the tangential mean the cases that the incident neutrons enter along the radial and tangential directions of the cylindrical cell, respectively. All measurements were performed at room temperature, T = 25 °C.

4. CV-SANS. For contrast-variation SANS (CV-SANS), a series of samples with different scattering length densities of solvent were prepared. The scattering length densities were calculated on the basis of their chemical structures and mass densities. The densities of clay and PEO are 2.65 and 1.13 g/mol, respectively. Figure 3 shows the variations of the scattering length densities (SLD; ρ_i) of clay, PEO, and the solvent as a function of deuterated water fraction, f_{D_2O}. Though ρ_{PEO} is independent of f_{D_2O}, ρ_{clay} linearly increases with f_{D_2O} due to D/H substitution of the hydroxyl group on the clay surface as extensively discussed elsewhere. The CV-SANS measurement was carried out with some D_2O fractions (f_{D_2O} = 0, 0.6, 0.7, 0.8, 0.9, and 1.0), where the measuring points are marked by filled circles.

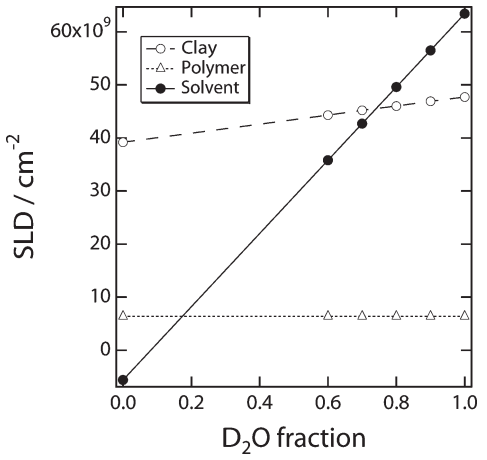

Figure 3. Scattering length densities of water (solid line with filled circles), clay (dashed line with open circles), and PEO (dotted line with open triangles) as a function of D_2O fraction in aqueous solution, f_{D_2O}. Each symbol indicates experimental condition on the line, i.e., $f_{D_2O} = 0$, 0.6, 0.7, 0.8, 0.9, and 1.0.

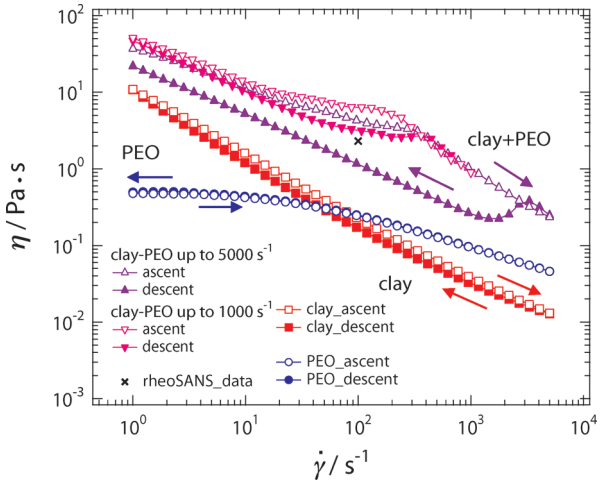

Figure 4. Shear rate dependence of viscosity on 3 wt % clay dispersion (square), 2 wt % PEO solution (circle), and the mixed solution (triangle and inverted-triangle) during ascent (open symbol) and descent (occupied symbol) processes. Data were taken with the cone-and-plate geometry. The viscosity of the mixed solution at $\dot{\gamma} = 100\ s^{-1}$ double cylinder is also shown with the black cross.

Results and Discussion

1. Overview of the Rheological and SANS Behavior. Figure 4 shows the variation of viscosities of (a) clay dispersion in water, (b) PEO aqueous solution, and (c) PEO−clay mixture in water taken with the cone-and-plate geometry. The ascent and descent processes up to 5000 (triangle) and 1000 s^{-1} (inverted-triangle) are denoted with open and closed symbols. Note that PEO solutions do not exhibit any hysteresis loop and simply show a shear-thinning behavior, typical for polymer solutions. Though the clay dispersant also does not have any hysteresis, its rheological behavior is markedly different from that of PEO solutions. This behavior is interpreted as destruction/formation of card-of-house structure characteristic of clay.[30−32] The strong reproducibility is due to electrostatic interactions between clay platelets, i.e., positive charge on the edge and negative charge on the plane surface. Interestingly, a simple mixing of the two systems results in a remarkable increase in the viscosity and a route-dependent viscosity behavior with respect to the shear rate, $\dot{\gamma}$. In order to elucidate these unique rheological behaviors, we carried out rheo-SANS experiments. In-situ rheo-SANS

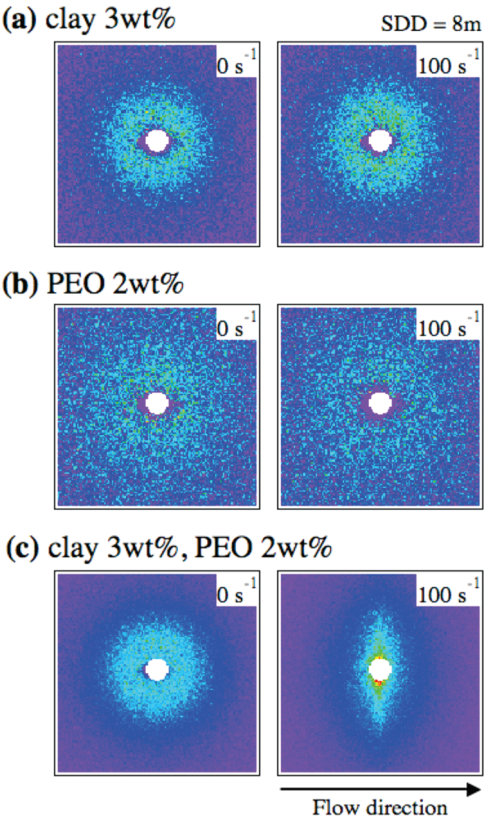

Figure 5. SANS 2D profiles of (a) clay dispersion, (b) PEO solution, and (c) the mixed solution in a stationary (0 s^{-1}) and flow (100 s^{-1}) states.

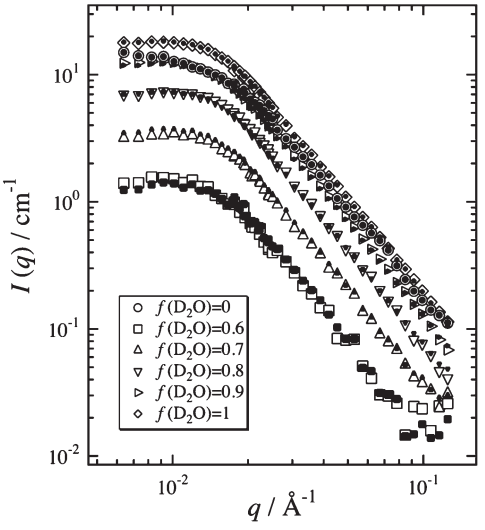

Figure 6. Scattering intensities of a clay−PEO mixed solution obtained for the different D_2O fraction in a stationary state (0 s^{-1}). Open symbols and occupied symbols indicate experimental and reconstructed values from decomposed partial scattering function.

experiments were carried out with increasing shear rate. It should be noted the following. Even though the clay−PEO mixed solution exhibits a hysteresis behavior, the initial rheological properties were recovered within 10 min. Hence, we believe that the hysteresis does not affect the experimental result. The viscosity was a decreasing function of up to 5000 s^{-1}. However, when the shear rate was decreased, a stepwise drop in η was observed, followed by a gradual increase as shown in filled triangles. This is probably due to the structural relaxation after release of high shear. This result shows that by high shear deformation PEO

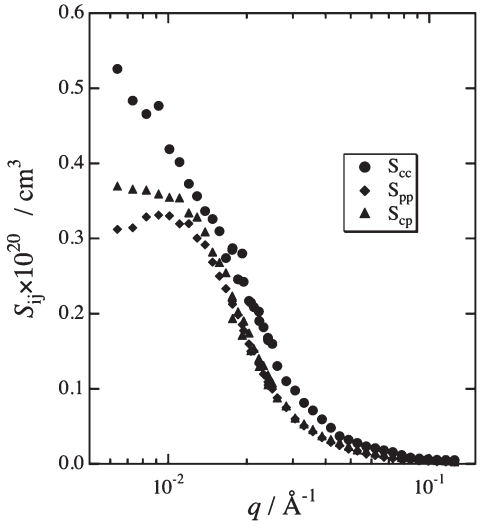

Figure 7. Obtained partial scattering functions of clay, S_{CC} (filled circle), PEO, S_{PP} (filled diamond), and clay−PEO cross-term, S_{CP} (filled triangle), in a stationary state.

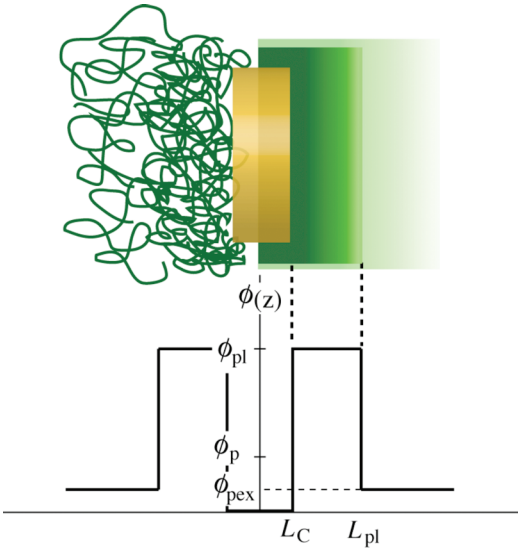

Figure 8. Polymer density profile perpendicular to the clay surface and model illustration (upper). Here ϕ_p, ϕ_{pl}, and ϕ_{pex} denote polymer volume fraction of a whole (as preparation), polymer layer on the clay surface, and nonadsorbed external polymer chains, respectively.

chains are stretched and bridge between clay particles. The validity of this speculation is confirmed by the hysteresis loop experiment up to $\dot{\gamma} = 1000\ s^{-1}$ (inverted triangles). The black cross at $\dot{\gamma} = 100\ s^{-1}$ in Figure 4 shows the viscosity change of clay + PEO with shear rate observed with double-cylinder rheometer. As shown here, the result is quite consistent with those observed by cone-and-plate geometry, and no hysteresis was observed as far as the highest shear rate was low enough (i.e., $\dot{\gamma} \approx 100\ s^{-1}$).

Figure 5 shows the SANS patterns for (a) clay dispersion, (b) PEO solutions, and (c) a mixture of clay and PEO measured at $f_{D_2O} = 1.00$. The patterns in the left and right columns were obtained without ($\dot{\gamma} = 0\ s^{-1}$) and with shear ($\dot{\gamma} = 100\ s^{-1}$), respectively. Note that only the mixture (c) shows an anisotropic pattern, i.e., a prolate pattern elongated in the perpendicular direction to the flow direction. An anisotropic pattern was also expected in the clay dispersion (a) due to a preferential orientation of clay platelets by flow. As a matter of fact, however, the pattern was isotropic. This result agrees with those as reported by Schmidt et al.,[17] indicating that such orientation does not occur and the platelets undergo turbulent motion by shearing. The SANS pattern for PEO (b) also suggests that the shear rate of $\dot{\gamma} = 100\ s^{-1}$ is not large enough to lead to shear-induced orientation of polymer chains. This type of anisotropic patterns were also observed by Loizou et al. in PEO and clay aqueous mixtures.[20] They carried out a series of measurements by varying the shear rate as well as the molecular weight of PEO. As shown in Figure 5 of ref 20, anisotropic patterns appear by increasing shear rate or by increasing molecular weight. They did not observe an anisotropic patterns for $\dot{\gamma} = 30\ s^{-1}$ but for $\dot{\gamma} = 90\ s^{-1}$ for PEO with the molecular weight of 100 kg/mol. Hence, the agreement between their result and in this work is quite satisfactory. According to the result of Loizou et al., it is clear that the isotropic−anisotropic transition is gradual with respect to the shear rate as well as the PEO molecular weight. Therefore, the comparison of the SANS data at zero shear and a high shear at which anisotropic pattern appeared is enough for general discussion of the origin of the anisotropic pattern.

2. Contrast-Variation SANS for Samples in a Stationary State. Figure 6 shows the SANS intensity functions obtained without shearing (i.e., $\dot{\gamma} = 0$). The open and solid symbols denote the observed and the reconstructed curves by CV procedure, respectively. As shown clearly in the figure, each of the reconstructed scattering intensity function well reproduces the corresponding observed SANS function, indicating that the CV procedure is quite successful.

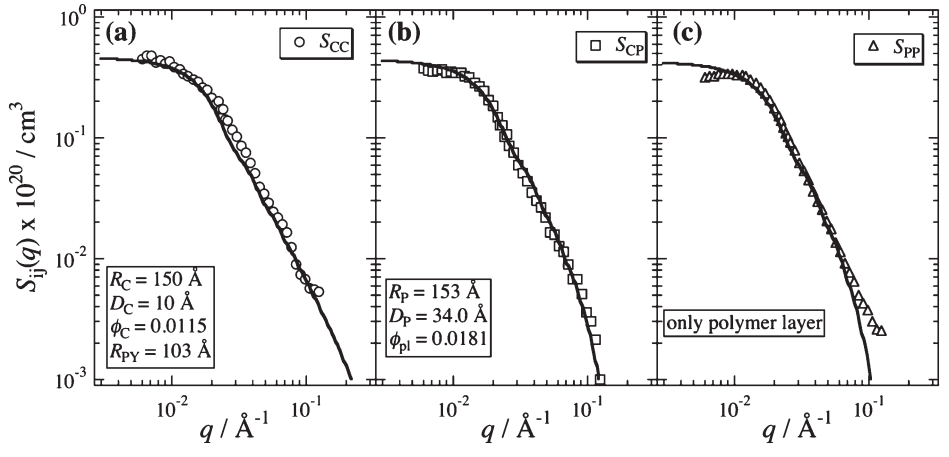

Figure 9. Partial scattering functions for clay−PEO mixed solution in a stationary state. Solid lines are the fitting curves by eqs 5, 6, and 7.

The resultant partial structure factors, $S_{ii}(q)$, are shown in Figure 7. Though all factors are decreasing functions of q, particularly for $q \geq 0.02$ Å^{-1}, the sign of $S_{CP}(q)$ being positive and the presence of maximum in $S_{PP}(q)$ are significant features of the system. The former suggests the presence of strong affinity between P (PEO) and C (clay), indicating that PEO chains are strongly adsorbed on clay surface. The latter, on the other hand, results in a constructive interference between the adsorbed layers across a clay platelet, resulting in a maximum in $S_{PP}(q)$.

In order to confirm this conjecture, we carried out curve fitting of the SANS curves with model functions. Figure 8 shows a disk model with polymer-adsorbed layer. For simplicity, the adsorbed layer is described by a disk-shape shell with a sharp boundary. The thickness of the shell is ($D_{pl} - D_C$), and the local polymer volume fraction near the surface of clay (i.e., the polymer concentration) is ϕ_{pl}. The local polymer volume fractions in a solution (without adsorbed polymer) after polymer adsorption are given by ϕ_{pex}. The total polymer volume fraction is ϕ_p ($= \phi_{pl} + \phi_{pex}$). The fitting functions are the same as those employed by Miyazaki et al.[25] an Endo et al.[22]

Figure 9 shows the results of curve fitting for $S_{ii}(q)$'s without shearing (i.e., $\dot{\gamma} = 0$). The parameters used for fitting are also shown in the figure. The radius and the thickness of clay platelet were fixed to be 150 and 10 Å, respectively. The clay volume fraction was the same as the stoichiometrical value. Here, we introduce a Percus−Yevick type structure factor to reproduce a suppression of $S_{CC}(q)$ by interplatelet interference. In $S_{CP}(q)$, the radius and the thickness of the outer shell consisting of adsorbed polymer chains are evaluated to be 153 and 34 Å, respectively. As a result of adsorption, the local polymer concentration was increased to 0.39 from 0.0181. $S_{PP}(q)$ was reproduced by simply using the adsorbed polymer layers. The positive deviation of the curve-fitted curve at low q may indicate the presence of interlayer interaction and needs further refinement. Here, the contribution of the scattering from the polymer matrix, i.e., the last term of the right-hand side of eq 7, was found to be negligible.

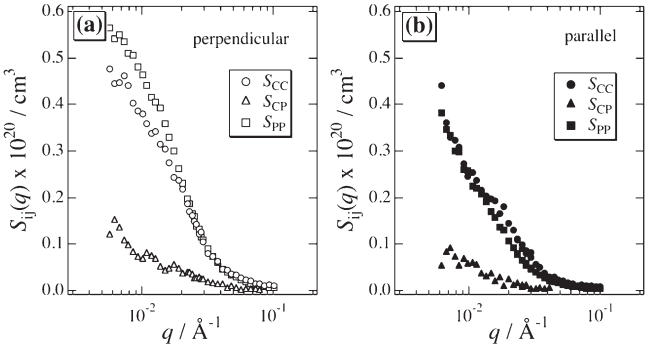

Figure 10. Partial scattering functions which averaged with sector area (±20°) in a flow field ($\dot{\gamma} = 100$ s^{-1}).

3. Contrast-Variation SANS for Samples in a Flow Field. In order to understand the rheological behavior in a flow field (Figure 4), we carried out rheo-SANS on the clay−PEO systems in a flow field, followed by contrast variation. Figure 10 shows $S_{ii}(q)$'s with sector average (±20°) in the flow field with $\dot{\gamma} = 100$ s^{-1}. Several interesting features can be drawn from this figure. First of all, $S_{ij}(q)$'s are direction-oriented, indicating that all of $S_{CC}(q)$, $S_{PP}(q)$, and $S_{CP}(q)$ become anisotropic by shearing. Second, the cross-term, i.e., $S_{CP}(q)$, is markedly suppressed by shearing. This is a piece of direct evidence of desorption of PEO chains from clay surface.

Figure 11 shows the results of curve fitting for the clay−PEO systems in the flow field. The curve fitting was conducted by the following procedure. Fitting of $S_{CC}(q)$ was done with a randomly oriented disk scattering function. After fixing the fitting parameters (α_C, $R_{PY\parallel}$, $R_{PY\perp}$), fitting of $S_{CP}(q)$ was conducted to evaluate R_P, D_P, and ϕ_{pl}. Then, the values of $\xi_\parallel$ and $\xi_\perp$ were obtained by fitting $S_{PP}(q)$. Now, the Percus−Yevick thickness becomes anisotropic. From Figure 11a (i.e., $S_{CC}(q)$), we learn that the allowance angle of clay orientation becomes smaller ($\alpha_C = 18.8°$: a preferred orientation between $18.8° \leq \alpha \leq 90°$) from $\alpha_C = 0°$ (i.e., random orientation between $0° \leq \alpha \leq 90°$). This preferred orientation is qualitatively similar to those reported by Loizou et al.[20] However, it should be noted here that the Herman parameter is originally introduced to discuss crystal orientation and the corresponding diffraction peak should be sharp enough with respect to the azimuthal angle. Therefore, the Herman orientation factor discussed in the paper by Loizou cannot be uniquely determined since the SANS functions are too broad to apply the Herman's parameter. $S_{CP}(q)$ shows that the polymer layer becomes more flat (from 153 to 196 Å in radius and from 34 to 25 Å in thickness) and the local polymer concentration decreases (from 0.39 to 0.094) by shearing. From Figure 11c, it is clear that the PEO chains are elongated along the flow direction, resulting in anisotropic blob formation with $\xi_\parallel = 131$ Å and $\xi_\perp = 77$ Å. The dashed lines indicate the scattering intensity contribution

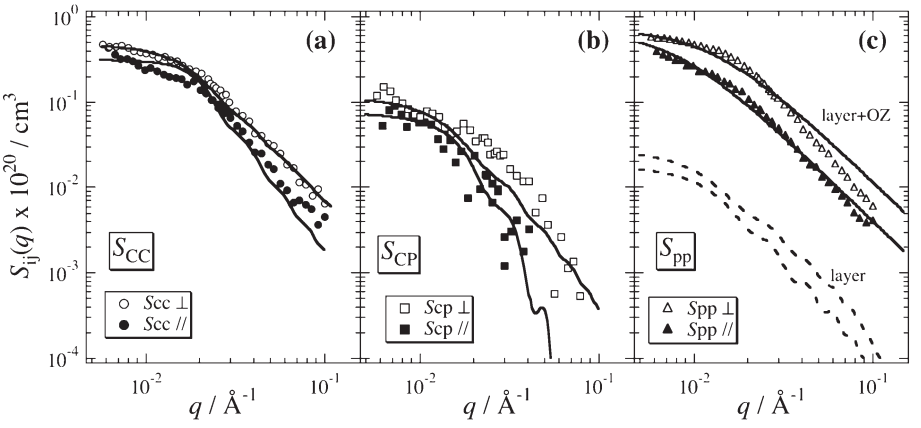

Figure 11. Partial scattering functions in a flow field and the fitting results. Open symbols and closed symbols show the perpendicular and parallel direction to the flow, respectively. Solid lines are the fitting results. The dashed lines indicate the scattering intensity contribution from the adsorbed polymer layer.

Table 1. Fitting Parameters on a Clay−PEO Mixture Solution under Shear Deformation

parameters		0 s^{-1}	shear rate	100 s^{-1}
S_{CC}	R_C		150 Å (fixed)	
	D_C		10 Å (fixed)	
	ϕ_C		0.0115 (fixed)	
	α_C	0° (fixed)		18.8°
	$R_{PY\perp}$	103 Å		100 Å
	$R_{PY\parallel}$			121 Å
S_{CP}	ϕ_P		0.0181 (fixed)	
	R_P	153 Å		196 Å
	D_P	34 Å		25 Å
	ϕpl	0.39		0.094
S_{PP}	$\xi_\perp$			77 Å
	$\xi_\parallel$			131 Å

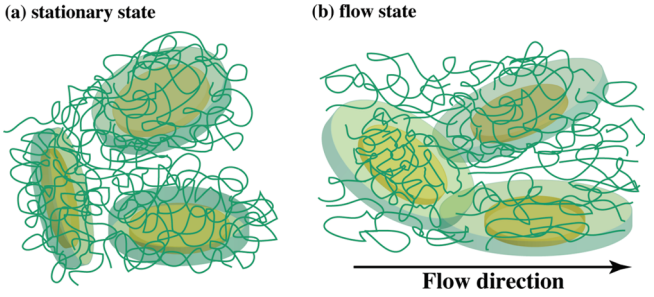

Figure 12. Model illustrations for the clay−PEO mixed solution (a) in a stationary (b) in a flow.

from the adsorbed polymer layer. Other fitting parameters together with those discussed above are listed in Table 1. Note we employed "global fitting" which requires least fitting errors for many scattering functions with a set of fitting parameters. This is why some fitting results do not look satisfactory. However, as it should be, the fitting parameters should be valid for each scattering function, and the result listed in Table 1 was the best in our analysis.

On the basis of the findings described above, we now propose a deformation model of clay−PEO mixtures in aqueous solutions. Figure 12 shows schematic models of the deformation model. In a stationary state, a significant amount of PEO chains is adsorbed on the clay surface (indicated with a darker color). Because of the presence of tie-chains bridging neighboring clay platelets, the viscosity is higher than that of clay dispersion without PEO chains (see Figure 4). When the system is sheared, the adsorbed layer is destroyed and desorption occurs. However, by reducing the shear rate, polymer chains start to adsorb on the clay platelets again. Here, the desorption/adsorption process is very much dependent on the history of shearing, leading to a strong hysteresis behavior (see Figure 4). The viscosity-thinning behavior discussed in this work is observed in a range with relatively high polymer concentration. Interestingly, a viscosity thickening instead of viscosity thinning is observed when the polymer concentration is decreased. Investigation on the structure−rheological behavior in such a region is another topic, which will be reported in the forthcoming paper.

Conclusion

The microscopic structure of clay−PEO mixed solution under steady shear field has been investigated by contrast-variation small-angle neutron scattering coupled with rheological measurements, i.e., rheo-SANS. The following facts are disclosed: (1) By adding PEO to clay suspension, the rheological behavior drastically changed, i.e., viscosity increases and hysteresis appears. (2) Under a flow field, only the mixture of clay and PEO shows an anisotropic pattern. (3) In the stationary state, an attractive interaction exists between PEO chains and clay platelets. This suggests that PEO chains are concentrated on a surface of clay. (4) By decomposition of scattering intensities in a shear state, it is found that PEO chains adsorbed on a clay surface are peeled off. The thickness of the adsorbed layer changes from 34 to 24 Å by shearing with $\dot{\gamma} = 100\ s^{-1}$. Furthermore, the clay platelets become oriented in the angular range of ca. 20°−90°, i.e., a preferential perpendicular orientation with its disk axis parallel to the vorticity direction. The PEO chains suspended in the solution are highly elongated by shear deformation. As a result, shear-thinning behavior is observed accompanied by a hysteresis loop in the process of increasing and decreasing shear rates.

Acknowledgment. This work was partially supported by the Ministry of Education, Science, Sports and Culture, Japan (Grants-in-Aid for Scientific Research (A), 2006−2008, no. 18205025, and for Scientific Research on Priority Areas, 2006−2010, no. 18068004). The SANS experiment was performed with the approval of the Institute for Solid State Physics, The University of Tokyo (proposal no. 8620), at the Japan Atomic Energy Agency, Tokai, Japan.

References and Notes

(1) Otsubo, Y.; Umeya, K. *J. Rheol.* **1984**, *28*, 95–108.
(2) Butera, R. J.; Wolfe, M. S.; Bender, J.; Wagner, N. J. *Phys. Rev. Lett.* **1996**, *77* (10), 2117–2120.
(3) Shibayama, M.; Kawada, H.; Kume, T.; Sano, T.; Matsunaga, T.; Osaka, N.; Miyazaki, S.; Okabe, S.; Endo, H. *J. Chem. Phys.* **2007**, *127*, 144507.
(4) Usuki, A.; Kojima, Y.; Kawasumi, M. *J. Mater. Res.* **1993**, *8*, 1179–1184.
(5) Kojima, Y.; Usuki, A.; Kawasumi, M. *J. Mater. Res.* **1993**, *8*, 983–986.
(6) Takayanagi, M.; Ogata, T.; Morikawa, M.; Kai, T. *J. Macromol. Sci., Part B* **1980**, *17* (4), 591–615.
(7) Haraguchi, K.; Takehisa, T. *Adv. Mater.* **2002**, *14*, 1120–1124.
(8) Haraguchi, K. *Curr. Opin. Solid State Mater. Sci.* **2007**, *11*, 47–54.
(9) Schmidt, P. S. G. *Colloid Polym. Sci.* **2009**, *287*, 1–11.
(10) Nelson, A.; Cosgrove, T. *Langmuir* **2004**, *20* (6), 2298–2304.
(11) Loiseau, A.; Tassin, J. F. *Macromolecules* **2006**, *39* (26), 9185–9191.
(12) Pozzo, D. C.; Walker, L. M. *Colloids Surf., A* **2004**, *240*, 187–198.
(13) De Lisi, R.; Gradzielski, M.; Lazzara, G.; Milioto, S.; Muratore, N.; Prévost, S. *J. Phys. Chem. B* **2008**, *112*, 9328–9336.
(14) Lal, J.; Auvray, L. *J. Appl. Crystallogr.* **2000**, *33*, 673–676.
(15) Lal, J.; Auvray, L. *Mol. Cryst. Liq. Cryst.* **2001**, *356*, 503–515.
(16) Schmidt, G.; Nakatani, A. I.; Butler, P. D.; Karim, A.; Han, C. C. *Macromolecules* **2000**, *33*, 7219–7222.
(17) Schmidt, G.; Nakatani, A. I.; Butler, P. D.; Han, C. C. *Macromolecules* **2002**, *35*, 4725–4732.
(18) Malwitz, M. M.; Butler, P. D.; Porcar, L.; Angelette, D. P.; Schmidt, G. *J. Polym. Sci., Part B: Polym. Phys.* **2004**, *42*, 3102–3112.
(19) Loizou, E.; Butler, P.; Porcar, L.; Schmidt, G. *Macromolecules* **2006**, *39* (4).
(20) Loizou, E.; Porcar, L.; Schexnailder, P.; Schmidt, G.; Butler, P. *Macromolecules* **2010**, *43*.
(21) Endo, H.; Schwahn, D.; Cölfen, J. *J. Chem. Phys.* **2004**, *120*, 9410–9423.
(22) Endo, H.; Miyazaki, S.; Haraguchi, K.; Shibayama, M. *Macromolecules* **2008**, *41*, 5406–5411.
(23) Nishida, T.; Endo, H.; Osaka, N.; Li, H.-J.; Haraguchi, K.; Shibayama, M. *Phys. Rev. E* **2009**, *80*, 030801.
(24) Shibayama, M.; Nomura, S.; Hashimoto, T.; Thomas, E. L. *J. Appl. Phys.* **1989**, *66*, 4188–4197.
(25) Miyazaki, S.; Endo, H.; Karino, T.; Haraguchi, K.; Shibayama, M. *Macromolecules* **2007**, *40*, 4287–4295.
(26) Percus, J. K.; Yevick, G. J. *Phys. Rev.* **1958**, *110*, 1–12.
(27) Mourchid, A.; Lécolier, E.; Van Damme, H.; Levitz, P. *Langmuir* **1998**, *14*, 4718–4723.

(28) Okabe, S.; Karino, T.; Nagao, M.; Watanabe, S.; Shibayama, M. *Nucl. Instrum. Methods Phys. Res., Sect. A* **2007**, *572*, 853–858.
(29) Okabe, S.; Nagao, M.; Karino, T.; Watanabe, S.; Adachi, T.; Shimizu, H.; Shibayama, M. *J. Appl. Crystallogr.* **2005**, *38*, 1035–1037.
(30) van Olphen, H. *Clay Colloid Chemistry*, 2nd ed.; John Wiley: New York, 1977.
(31) van Olpehn, H. *An Introduction to Clay Colloid Chemistry*; Wiley: New York, 1997.
(32) Pignon, F.; Magnin, A.; Piau, J.-M. *J. Rheol.* **1998**, *42*, 1349–1371.